



TECHNICAL ARTICLE

Influence of Cooling Rate on Solidification and Segregation Characteristics of Cu-Ni-Si Alloy

Guangming Cao, Ruixiang Li, Shuang Zhang, Hao Wang, and Yuanxiang Zhang

Submitted: 22 June 2022 / Revised: 13 February 2023 / Accepted: 27 February 2023 / Published online: 13 March 2023

Differential scanning calorimetry (DSC) and confocal scanning laser microscopy (CSLM) were used to investigate the effects of different cooling rates on the solidification and segregation characteristics of Cu-Ni-Si alloy. The microstructures were characterized by electron probe microanalysis and scanning electron microscope. The effects of cooling rate on segregation degree, grain size, solidification temperature and secondary dendrite spacing (λ_2) were analyzed, and the correlation function was established. The results show that the characteristic temperature of DSC phase transformation is similar to the characteristic temperature of CSLM in situ microstructure evolution. Increasing cooling rate can reduce segregation degree and refine grains. The relationships between cooling rate and crystallization temperature ($T_{L \rightarrow S}$) and secondary dendrite spacing (λ_2) with cooling rate are as follows: $T_{L \rightarrow S} = 176 \times \exp(-v/17.6) + 891$ and $\lambda_2 = 63 \times v^{-0.236}$, respectively. The above relations were applied to predict the solidification microstructure characteristics produced by twin-roll strip casting and ingot casting processes, and the predicted results are in good agreement with the experimental values. The advantages of grain refinement and segregation improvement and its optimization mechanism of twin-roll strip casting have been clarified.

Keywords Cu-6Ni-1.4Si alloy, CSLM, DSC, solidification, segregation

1. Introduction

As a high strength conductive material, Cu-Ni-Si has been widely used in various electronic products such as lead frame connection terminal and has a strong substitution effect on toxic beryllium-copper alloy (Ref 1-3). However, the harsh application environment has high requirements on the strength of the alloy; therefore, high alloying becomes an effective method. Besides, the segregation of the alloy under traditional casting is serious, and the coarse grain size is inevitable. Studies show that increasing cooling rate can effectively reduce segregation and refine grain (Ref 4, 5). Fortunately, compared with IC, TRSC has the characteristics of sub-rapid solidification (Ref 6). Cao et al. (Ref 7) found that the solidification microstructure of Cu-3.2Ni-0.75Si alloy could be refined by TRSC, and the average grain size of the cast band was significantly refined. Liu et al. (Ref 8) successfully prepared 17% Cr ferrite stainless steel (FSS) as cast zone by TRSC under different melt overheating conditions. The as-cast structure of FSS is composed of fine equiaxed and columnar crystals. Daamen et al. (Ref 9) also pointed out that TRSC is an option for producing TWIP steel with competitive tensile strength compared to TWIP steel obtained through conventional machining

methods. Pande et al. (Ref 10) concluded through research that primary dendrite arm and secondary dendrite spacing are related to cooling rate. Jabbari Behnam et al. (Ref 11) proposed that as cooling rate increases, the degree of undercooling increases, while the diffusion rate decreases.

However, few studies can quantitatively characterize the effect of cooling rate on the microstructure and characteristic temperature of solidification. Wielgosz and Kargul (Ref 12) used DSC to study the solid-liquid phase change of non-alloy peritectic steel at high temperature, and the results showed that the solid-phase line and liquidus temperature were in good agreement with the numerical calculation results. Miao et al. (Ref 13) proposed a CSLM solidification process for IN718 superalloy, which shows that this method has great potential for studying the solidification process. Hechu et al. (Ref 14) proposed a new method to explain the solidification behavior of peritectic steel by combining DSC and CSLM. The results show that the method can accurately control the solidification parameters and cooling rate. In conclusion, DSC can detect the solid-liquid phase change characteristics, and CSLM can characterize the in situ structure evolution during the melting and solidification of alloys at different speeds, which is an important means to explore the effect of cooling rate on the solidification process of alloys.

Compared with IC, TRSC has the characteristics of sub-rapid solidification, which can refine grains and inhibit segregation. However, in the process of IC or TRSC, the exact cooling rate is not given, and the effect of cooling rate on the inhibition of micro-segregation cannot be quantified. In this study, DSC and CSLM methods were introduced into the analysis of the solidification process of high alloyed copper alloy, systematically studied the effect of cooling rate on solidification microstructure, characteristic temperature and segregation behavior of high alloyed Cu-Ni-Si alloy and applied to TRSC and traditional casting process. By comparing

Guangming Cao, Ruixiang Li, Shuang Zhang, Hao Wang, and Yuanxiang Zhang, The State Key Lab of Rolling and Automation, Northeastern University, Shenyang 110819 Liaoning Province, People's Republic of China. Contact e-mail: caogm@ral.neu.edu.cn.

the prediction and experimental data, the sub-rapid solidification characteristics and casting advantages of TRSC were analyzed theoretically. It provides theoretical guidance for improving the solidification microstructure of alloy by controlling the cooling rate.

2. Experimental Materials and Methods

2.1 Material Preparation

The experimental materials were Cu-6Ni-1.4Si alloy prepared by IC and TRSC process. The mass fractions of components are: Ni: $6.0 \pm 0.1\%$, Si: $1.4 \pm 0.05\%$, $O \leq 0.006\%$, and the rest were Cu. The alloy was melted in the vacuum induction furnace, and the melting temperature is $1100 \sim 1300 \text{ }^\circ\text{C}$, and the melting process lasts about 60 min and then cast in the round iron mold where the casting temperature is about $1150 \text{ }^\circ\text{C}$. The mother alloy was remelted in a vacuum furnace, and then the strip was cast on an equal-diameter twin-roll strip caster at $1150 \text{ }^\circ\text{C}$ of casting temperature, where the 3-mm-thick and 110-mm-wide casting strip was prepared, and the casting and rolling speed was set as 30 m/min.

2.2 DSC and CSLM Experiments

DSC experiments were performed on a SETARAM SETSYS Evolution S60/58507 synchronous thermal analyzer test equipment. Specimens with 3 mm diameter and 3 mm height were prepared from the cast strip (CS). The experimental sample was placed in a corundum crucible of $\Phi 5 \times 4 \text{ mm}$, and the comparison sample was an empty corundum crucible. Then, put them in the equipment together. After vacuuming, the system was filled with argon and operated repeatedly for three times. The sample was subjected to the following heating and cooling cycles: room temperature \rightarrow heating at $0.1 \text{ }^\circ\text{C/s}$ to $1150 \text{ }^\circ\text{C}$ \rightarrow isothermal holding at $1150 \text{ }^\circ\text{C}$ for 180 s \rightarrow cooling at $0.1 \text{ }^\circ\text{C/s}$ to room temperature. In order to accurately control the cooling rate, this experiment uses high-purity helium as the cooling gas. To ensure the accuracy of the experimental results, three groups of parallel experiments were repeated.

CSLM experiments were performed on a VL2000DX-SVF17SP & 15FTC CSLM instrument. Specimens with 5 mm diameter and 3 mm height were prepared from the cast strip. Before each experiment, the air in the chamber system was evacuated, so argon was repeatedly filled three times to remove as much air as possible. The specimen was subjected to heating and cooling cycles as follows: room temperature \rightarrow heating at $8 \text{ }^\circ\text{C/s}$ up to $1100 \text{ }^\circ\text{C}$ \rightarrow heating at $2 \text{ }^\circ\text{C/s}$ up to $1150 \text{ }^\circ\text{C}$ \rightarrow isothermal holding at $1150 \text{ }^\circ\text{C}$ for 3 min \rightarrow cooling under different rates down to room temperature. The cooling rates were 0.1, 1, 10 and $100 \text{ }^\circ\text{C/s}$, respectively, as shown in Fig. 1. In order to accurately control the cooling rate, high-purity helium gas was used as the cooling gas in this experiment. The experiments were carried out through surface visualization of the specimens during heating and cooling processes. Enough images were recorded at 1-15 frames per second according to the varied cooling rates. The initial melting temperature and crystallization temperature were determined according to the tissue observation in situ. Besides, the IPP (Image pro plus) software was used to measure the

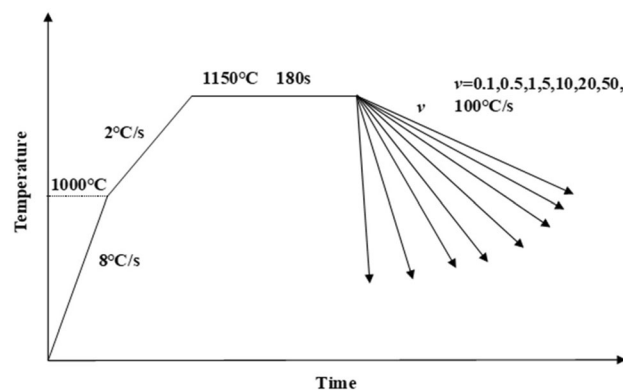


Fig. 1 Routing of cooling processes in CSLM experiments

secondary dendrite spacing of ingot and strip solidification structure.

2.3 Microstructural Analyses

All samples were metallographically prepared and then etched with a solution of 8 g $\text{FeCl}_3 + 20\text{mLHCl} + 100\text{mLH}_2\text{O}$ for 10 s. Olympus optical microscopy (OM) was used to observe microstructural features. Element segregation behavior was observed in a JEOL JXA-8530F electron probe micro-analyzer, and chemical compositions in dendrite arm and interdendritic region were measured by energy diffraction spectrum (EDS) and EPMA. The average value of 30 continuous points was taken as the final experimental value to ensure the smooth operation of the experiment. Also, map scanning with a step size of $0.2 \mu\text{m}$ was used to characterize the distribution of alloying elements.

3. Experiment Results

3.1 DSC Experimental Curve and Solidification Microstructure Analysis

DSC characterizes the occurrence of phase transition by heat flow changes. Heat flow deviation from baseline indicates that the solid-liquid phase transition begins to occur. During melting, the alloy absorbs latent heat of phase transition, and during solidification, the alloy releases latent heat of crystallization, resulting in heat flow deviation from baseline and the formation of heat flow peak (Ref 15). As shown in Fig. 2(a) and (b), the curve deviated from the baseline at $1048 \text{ }^\circ\text{C}$, and the alloy began to melt, arrived peak at $1100 \text{ }^\circ\text{C}$, indicating that the alloy had completely melted. The same goes for solidification. The initial melting temperature and final melting temperature of the alloy are 1048 and $1100 \text{ }^\circ\text{C}$, respectively. The initial and final solidification temperatures are 1077 and $1057 \text{ }^\circ\text{C}$, respectively.

Figure 2(c), (d), (e) and (f) shows the solidification structure and energy spectrum analysis results of DSC experimental samples. Figure 2(c) shows the metallographic microstructure of DSC test sample. The solidification structure consists of coarse dendrite structure, and the average secondary dendrite spacing is about $110 \mu\text{m}$. Figure 2(d) shows the EPMA morphology of the solidified structure, and obvious dendrite grain boundaries can be observed. Enlarge partial view of point

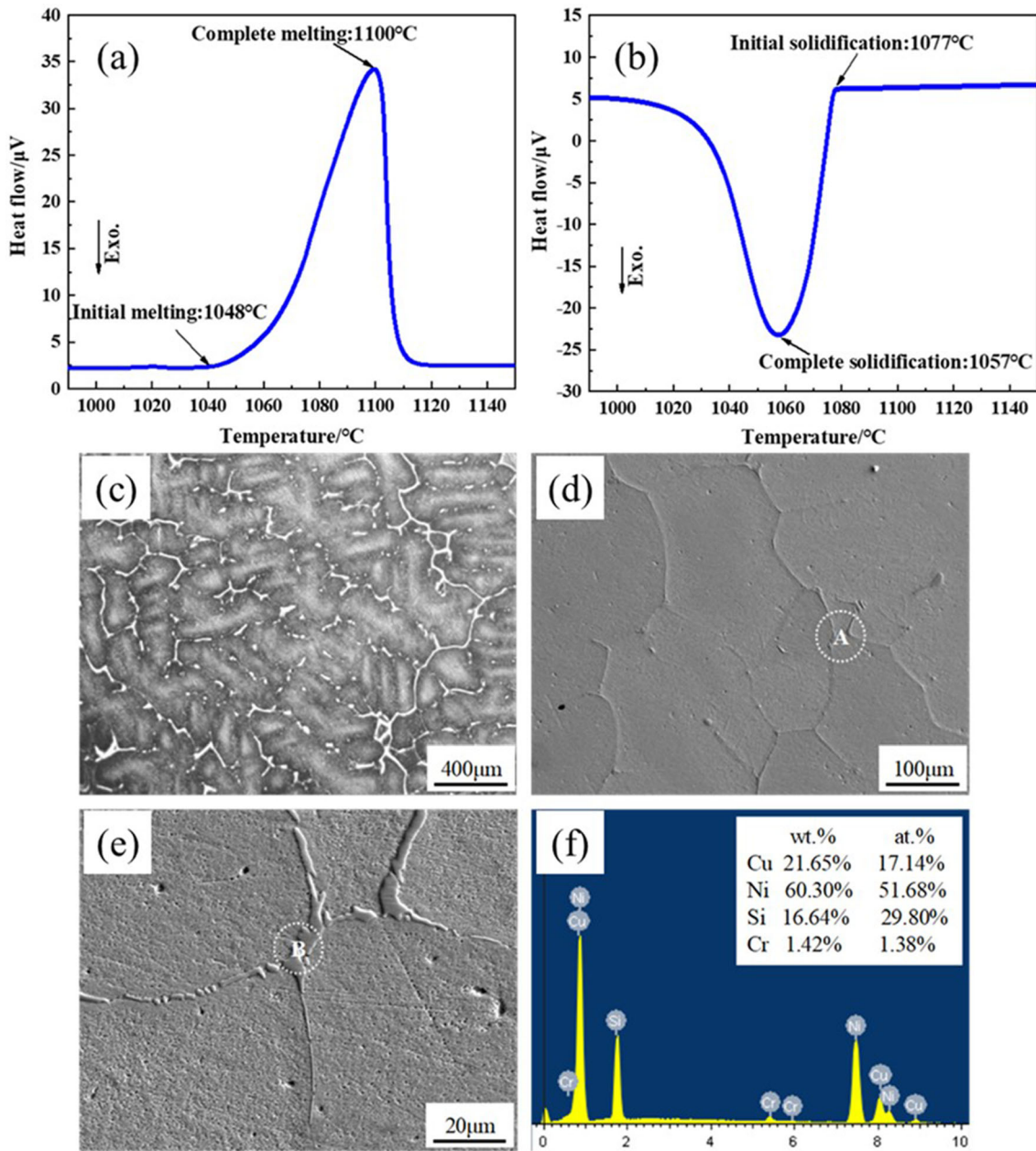


Fig. 2 Experimental curve obtained in DSC experiment and solidification structure and EDS result of DSC specimen. (a) Heating curve; (b) cooling curve; (c) metallographic structure; (d) EPMA morphology; (e) enlarged partial view of point A; (f) B point energy spectrum results

A, obvious grain boundary segregation can be observed at the grain boundaries, as shown in Fig. 2(e). As shown in Fig. 2(f), the composition of point B was determined through EDS, and the content of Ni, Si was large, intermetallic compounds were formed at the grain boundary, and segregation was serious; these phenomena are correspondent with Cheng et al. reported (Ref 16).

3.2 In situ Microstructures Upon Cooling Process of CSLM

Figure 3 shows the in situ observation of the microstructure evolution of Cu-6Ni-1.4Si alloy during melting and solidification at the cooling rate of 10 °C/s. As can be seen from the figure, when the sample is heated to 1091 °C, the surface of the sample begins to melt, as shown in Fig. 3(b), the temperature continues to rise, and the sample began to melt slowly. After

heated to 1150 °C, the sample melted completely, as shown in Fig. 3(d). After holding for 180 s, the molten liquid alloy is cooled at a cooling rate of 10 °C/s. When the liquid alloy is supercooled below the melting point, solidification occurs. The alloy begins to nucleate at 992 °C and this temperature is taken as the crystallization temperature of the alloy. When the temperature drops from 992 to 977 °C, the number of crystal nuclei increases significantly and part of crystal nuclei gradually grow up. When the temperature continues to decrease to 969 °C, crystal nuclei grow into dendrite structure, and the residual liquid phase is separated in the dendrite interval, as shown in Fig. 3(h). As the temperature was further reduced to 957 °C, the liquid phase was completely eliminated and the alloy was completely solidified. The solidification structure of the alloy presented a dendrite network structure, as shown in

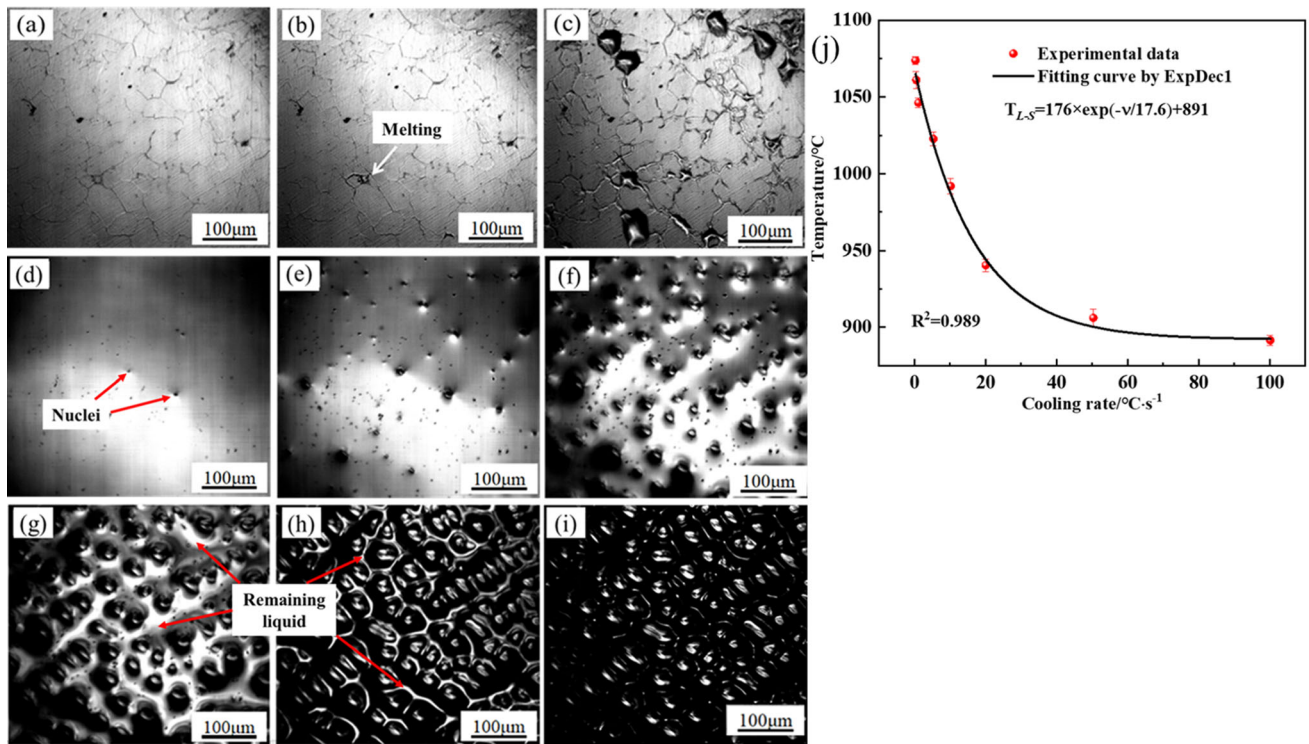


Fig. 3 CSLM in situ observation of melting and solidification process of alloy at cooling rate of 10 °C/s and correlation curve. (a) 1081 °C; (b) 1091 °C; (c) 1115 °C; (d) 992 °C; (e) 986 °C; (f) 977 °C; (g) 969 °C; (h) 957 °C; (i) 943 °C; (j) relationship curve between crystallization temperature and cooling rate

Fig. 3(f). In the solidification process, there is residual liquid phase in the early formed dendrite, which is the region where segregation takes place. Phase transition sequence during solidification: $L \rightarrow L + \alpha \rightarrow L + \alpha + \text{intermetallic} \rightarrow \alpha + \text{intermetallic}$, where α means copper phase; L represents liquid phase.

Figure 3(j) shows the corresponding crystallization temperatures under different cooling rates, namely the temperature of initiation of nucleation. As can be seen from Fig. 3(j), the crystallization temperature gradually decreases with the increase of cooling rate. ExpDec1 function is used to fit the relationship between them (Ref 17), and the following expression is obtained:

$$TL \rightarrow S = 176 \times \exp(v/17.6) + 891 \quad (\text{Eq 1})$$

where $TL \rightarrow S$ is the crystallization temperature, °C; v is cooling rate, °C/s.

During the cooling process, the crystallization temperature measured by DSC experiment is about 1077 °C. The crystallization temperature calculated by Eq 1 of CSLM experiment at 0.1 °C/s was 1074 °C, which was basically consistent with the crystallization temperature measured by DSC experiment. The characteristic temperatures about different rates under heating and cooling process are shown in Table 1.

3.3 Effect of Cooling Rate on the Solidification Microstructures

Figure 4 is the metallographic photographs of solidification structure under different cooling rates. It can be seen from the figure that the solidified structure is composed of dendritic structures with uniform size and then decreases with the

increase of cooling rate. The secondary dendrite spacing of solidification structure at different cooling rates was measured by IPP software. Taking the metallographic specimens with cooling rates of 0.1, 1, 10 and 100 °C/s as examples, the average secondary dendrite arm spacings are 109.29, 61.02, 37.09 and 25.32 μm , respectively.

Figure 4(e) shows the secondary dendrite spacing (SDAS, the value of SDAS is also described as λ_2 here) at different cooling rates. It can be seen from the figure that with the increase of cooling rate, λ_2 decreases, and the decrease rate is first fast and then slow. The transition temperature was about 10 °C/s. It is widely accepted that the relationship between λ_2 and cooling rate can be described as $\lambda_2 = K \times v^{-n}$. K and n are material constants; v is the cooling rate. As summarized and listed in Table 2, the values of these constants are variable for different materials. Based on the expression discussed above, data fitting analysis was performed on the relationship between λ_2 and v , which K and n were 63 and 0.236. Therefore, the relationship between λ_2 and v was expressed as follows (Ref 18):

$$\lambda_2 = 63 \times v^{-0.236} \quad (\text{Eq 2})$$

As indicated in Fig. 4, the average secondary dendrite spacing is about 110 μm . The cooling rate can be calculated by Eq 2. And the cooling rate got from Eq 2 was used to calculate the solidification temperature through Eq 1. The result is correspondent with the temperature got from DSC experiment.

3.4 Effect of Cooling Rate on Distribution of Alloying Elements

The cooling rate during solidification determines the segregation degree of the alloy, and the segregation degree

Table 1 Characteristic temperatures in the processes of DSC and CSLM experiments

Experiments	Heating process		Cooling process	
	Rate, °C/s	$T_{S \rightarrow L}$, °C	Rate, °C/s	$T_{L \rightarrow S}$, °C
DSC	0.1	1048	0.1	1077
CSLM	2	1091	0.1 ~ 100	$T_{L \rightarrow S} = 176 \times \exp(-v/17.6) + 891$

$T_{S \rightarrow L}$ is the starting melting temperature, °C; $T_{L \rightarrow S}$ is crystallization temperature, °C; v is cooling rate, °C/s

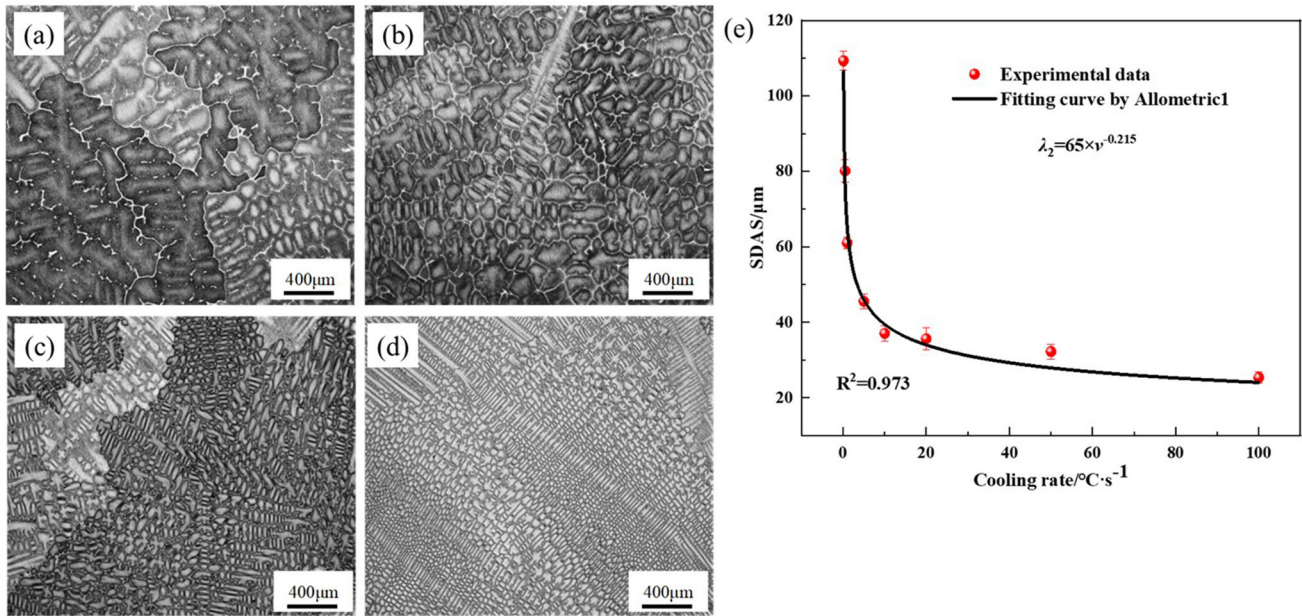


Fig. 4 Metallographic photographs of CSLM specimens at different cooling rates and correlation curve. (a) 0.1 °C/s; (b) 1 °C/s; (c) 10 °C/s; (d) 100 °C/s; (e) relationship curve between secondary dendrite arm spacing and cooling rate in CSLM specimens

Table 2 Values of K and n for different materials

Material	Condition	$K, \mu\text{m}^{n+1}\cdot\text{s}^{-n}$	n	References
Cu-6%Sn alloy	Melt droplet experiment	27	0.31	(Ref 18)
Fe-Cr-Ni-Mo-N SASS	DSC experiment	39	0.22	(Ref 17)
316L stainless steel	Welding experiment	25	0.28	(Ref 19)
Cu-6Ni-1.4Si alloy	CSLM experiment	63	0.236	This study

unusually determines the performance of the alloy. Therefore, it is of great significance to study the distribution of alloying elements in dendritic structures under different cooling rates. The segregation degree of alloy elements can be expressed by the dendritic segregation coefficient K , which is the ratio of the content of alloy elements in the inter-dendritic region (IDR) and the dendrite arm (DA) (Ref 17). The expression is as follows:

$$K = C_{IDR}/C_{DA} \quad (\text{Eq 3})$$

where K is segregation coefficient, the smaller $|K-1|$, the lighter segregation degree; C_{IDR} is the mass fraction of alloy elements in IDR, %; C_{DA} is the mass fraction of alloy elements in DA, %. The average contents of Cu, Ni and Si in IDR and DA of CSLM samples at different cooling rates were deter-

mined by EPMA, and the corresponding segregation coefficients were calculated. The results are shown in Table 3.

In order to further study the variation of segregation coefficient of alloy elements in CSLM samples under different cooling rates, the results in Table 3 are plotted as a diagram of the relationship between segregation coefficient and cooling rate, as shown in Fig. 5.

The diagram shows that the segregation coefficient of Cu is less than 1, indicating that it is enriched in DA, and the segregation coefficient of Ni and Si is greater than 1, indicating that it is enriched in IDR. With the increase of cooling rate, the segregation coefficient of Cu increases gradually, the segregation coefficient of Ni and Si decreases, and the absolute value of the difference with the mean 1 decreases gradually,

Table 3 Alloying element contents and their segregation coefficients in part of the CSLM specimens obtained at different cooling rates

$v, \text{ }^\circ\text{C/s}$		0.1	1	10	100
Cu	C_{IDR}	19.24	22.38	29.3	58.61
	C_{DA}	91.09	89.65	88.43	91.2
	K	0.21	0.25	0.33	0.64
Ni	C_{IDR}	62.31	58.79	52.9	29.65
	C_{DA}	7.26	8.47	9.6	6.95
	K	8.58	6.94	5.51	4.27
Si	C_{IDR}	16.67	17.13	16.25	10.86
	C_{DA}	1.65	1.88	1.97	1.85
	K	10.10	9.11	8.25	5.87

indicating that the degree of segregation decreases with the increase of cooling rate (Ref 17).

Figure 6 is the degree of element segregation in the solidification structure of CSLM samples at different cooling rates, mainly the surface scanning diagram of Ni and Si elements. It can be seen from the figure that with the increase of cooling rate, the segregation degree of Ni and Si elements is gradually reduced, which is corresponding to the calculation results of Fig. 5.

4. Discussion

4.1 Characteristic Temperature upon Heating and Cooling

Table 1 shows the characteristic temperature of melting and solidification process of Cu-6Ni-1.4Si alloy by DSC and CSLM. During the heating process, the initial melting temperature measured in DSC experiment was 1048 °C, and the average initial melting temperature measured in CSLM experiment was 1091 °C. There are two main reasons for the differences in the above results. On the one hand, the heating rate in DSC experiment was 0.1 °C/s. In CSLM experiment, it was first heated to 1000 °C at the heating rate of 8 °C/s and then 2 to 1150 °C. The faster the heating rate, the greater the superheat, and the higher the transition temperature from solid to liquid phase (Ref 20-23). On the other hand, the CSLM experiment is based on the observed melting phenomenon in the field of vision to determine the starting melting temperature. Due to the limitations of the observation area, other areas may have melted when the melting phenomenon is observed, resulting in a certain deviation. In addition, it is difficult to determine the exact starting and finishing points in CSLM experiment, compared to the DSC experiment. The reason is the promotion of phase transformation at the free surface through the relieving of strain effect and enhanced diffusion coefficient of solute elements.

Upon cooling process, crystallization temperature in DSC experiment was measured to be about 1077 °C. In this CSLM experiment, crystallization temperatures were as a function of cooling rate, which was expressed as $T_{\text{L} \rightarrow \text{S}} = 176 \times \exp(-v/17.6) + 891$. The crystallization temperature gradually decreases with the increase of cooling rate. It is well known that cooling rate has a significant effect on the crystallization temperature due to the liquid undercooling, which plays a central role in determining the solidification microstructures as

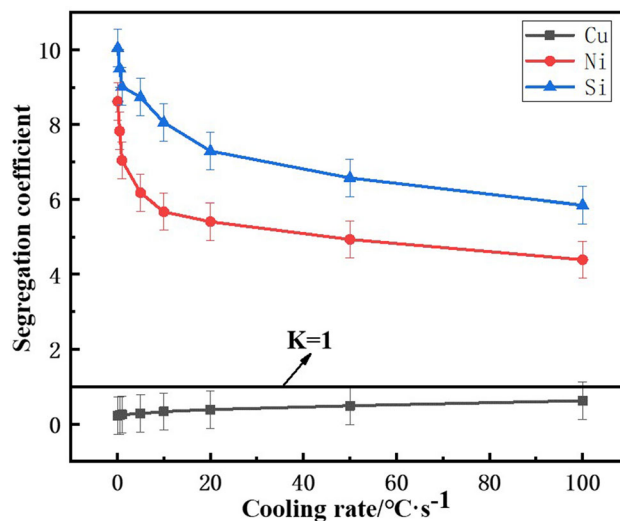


Fig. 5 Relationship between segregation coefficient of main alloying elements and cooling rate

Perepezko and Wilde reported 20. Also, Wielgosz et al. (Ref 24) indicated that higher cooling rate increases supercooling and further decreases solidification temperature.

4.2 Relationship Between Cooling Rate and Segregation

In order to establish a quantitative relationship between segregation cooling rate and segregation degree to predict the segregation degree of Cu-6Ni-1.4Si alloy at different cooling rates, based on the Clyne-Kurz model and consider the effects of multi-component, columnar dendrite structure, coarsening and other factors, Brody and Flemings (Ref 25) proposed an empirical formula for the relationship between cooling rate and segregation:

$$\beta = 2\alpha \left(1 - \exp\left(-\frac{1}{\alpha}\right) \right) - \exp\left(-2\frac{1}{\alpha}\right) \quad (\text{Eq 4})$$

$$\alpha = 2(\alpha_0 + \alpha^c) \quad (\text{Eq 5})$$

$$\alpha_0 = \frac{Kt_f}{x^2} \quad (\text{Eq 6})$$

$$x = \frac{\lambda_2}{2} \quad (\text{Eq 7})$$

$$t_f = \frac{T_{\text{liq}} - T_{\text{sol}}}{v} \quad (\text{Eq 8})$$

In order to calculate the anti-diffusion parameter β , the relationship between the segregation coefficient K and the cooling rate v needs to be calculated. Combined with Fig. 5, the data were fitted to obtain:

$$K_1 = 3.65 \exp(-v/24.18) + 5.93 \quad (\text{Eq 9})$$

$$K_2 = 3.89 \exp(-v/15.58) + 4.96 \quad (\text{Eq 10})$$

where α^c is 0.1, T_{liq} is 1100 °C and T_{sol} is 1057 °C according to Fig. 2. K_1 is the segregation of element Si; K_2 is the segregation of element Ni, which can be obtained from Table 3. β is back-diffusion parameter, α is Fourier number accounts for

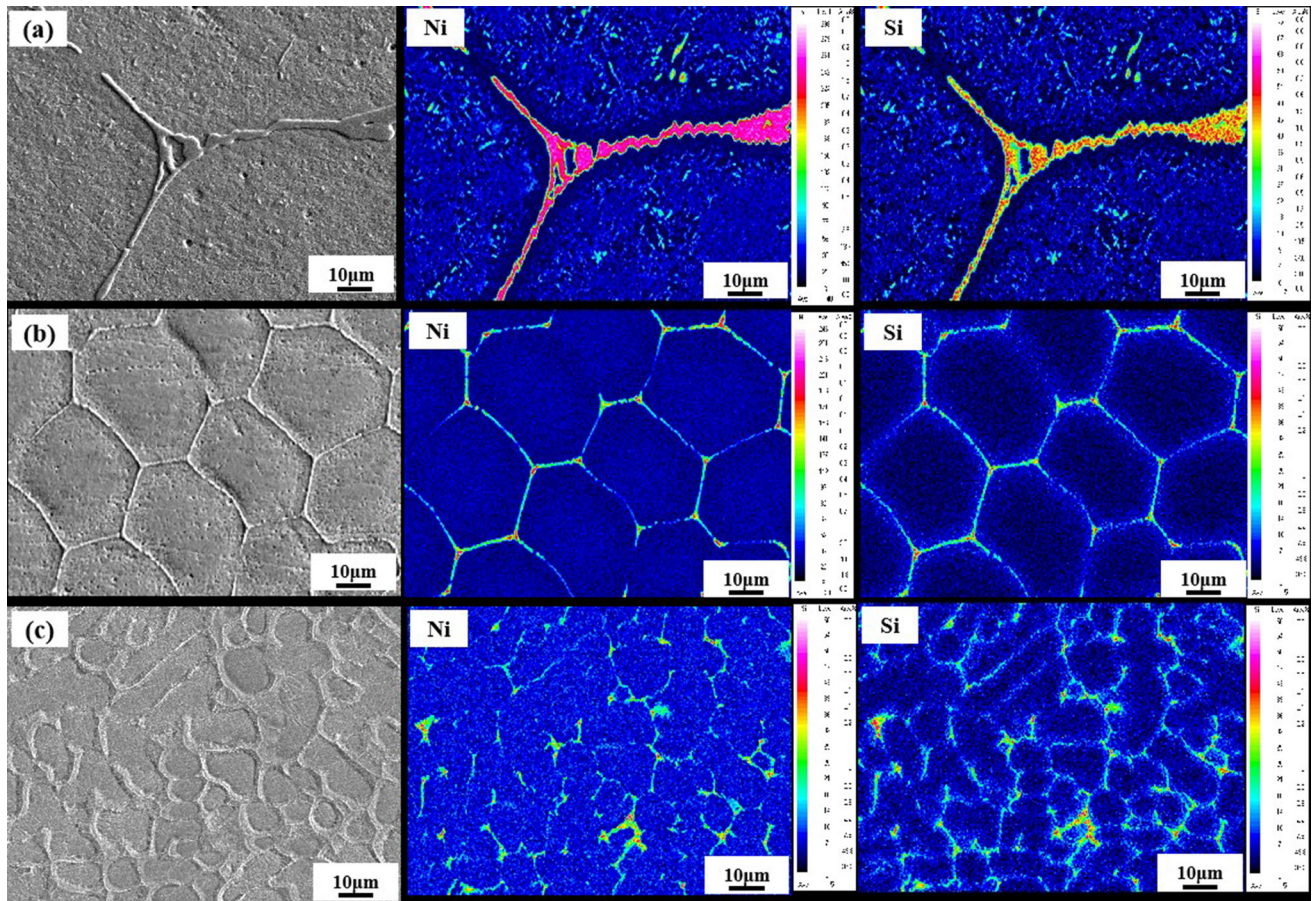


Fig. 6 Element segregation degree of CSLM samples at different cooling rates. (a) 0.1 °C/s; (b) 10 °C/s; (c) 100 °C/s

coarsening, α_0 is Fourier number. x is the width of the nodal area, which could be calculated by Eq 7 with Eq 2.

4.3 Application of This Research in IC and TRSC

The conclusions from DSC and CSLM experiments were applied to research the solidification and segregation characteristics in IC and TRSC. As shown in Fig. 7, the grain size of ingot solidification structure is relatively large. The internal grains show developed primary dendrite axis and secondary dendrite arm, and the secondary dendrite spacing is about 80 μm , and obvious segregation occurred. By contrast, the grains of the cast strip are finer and the dendrites are more dispersed.

From Fig. 7, the secondary dendrite spacing of ingot solidification structure was measured by IPP software to be in 70-90 μm , and the secondary dendrite spacing of strip solidification structure is in 6-15 μm . According to Eq 2, the cooling rate at any solidification region for the studied alloy can be calculated as long as λ_2 is given. The values of λ_2 in the ingot and CS in Fig. 7 were measured and are listed in Table 4. And the cooling rates were calculated as listed in Table 4. These results are well consistent with the common cognition and the results as Liu et al. reported (Ref 8).

The TSRC process is based on the sub-rapid solidification, and the cooling rate is unable to reach the equilibrium solidification condition, so the solidification process is still a non-equilibrium crystallization process (Ref 26). However, TSRC still provides its advantages. Figure 8 is the element

plane scan of ingot and CS produced by IC and TRSC, respectively. It can be seen from Fig. 8(a) that in the solidification structure of the ingot, Ni and Si elements are obviously enriched at the grain boundary of the dendrite. Compared with Fig. 8(b), it can be found that with the increase of cooling rate, the enrichment degree of Ni and Si elements at the grain boundary is significantly weakened. The above transformation is mainly due to the rapid cooling rate of TRSC, which makes the solid-liquid interface move rapidly in the process of melt solidification, and the local solidification time is very short. At the same time, the diffusion coefficient is reduced, and the solute retention phenomenon occurs when the alloy element is not as fast as the diffusion has been 'submerged' by the high-speed mobile interface, which greatly reduces the degree of element segregation of the alloy (Ref 27).

Solute partition coefficients k in as-cast microstructures of the ingot and CS were measured and compared to those in CSLM experiments, as indicated by ingot and CS in Fig. 5. Through the cooling rate information in Table 4, the anti-diffusion parameter β of elements Ni and Si in different casting processes was calculated through Eq. 4; the results show that the β under IC process is 0.671, and the β under TRSC is 0.056, which proves that TRSC significantly improves segregation. The values of k and β in ingot and CS conform to the law obtained by CSLM experiments. Based on the above analyses, the conclusions drawn from DSC and CSLM experiments are reliable to predict the solidification and segregation characteristics of the studies alloy.

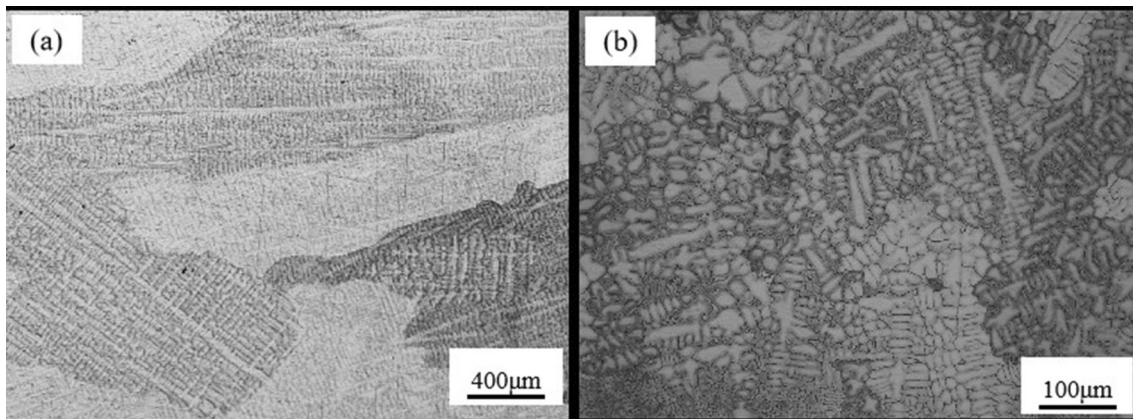


Fig. 7 Microstructure of ingot and casting strip. (a) Ingot; (b) cast strip

Table 4 Secondary dendrite spacing and cooling rate of solidification structure of ingot and cast strip

	$\lambda_s, \mu\text{m}$	$v, ^\circ\text{C}\cdot\text{s}^{-1}$
Ingot	70 ~ 90	0.22 ~ 0.71
Cast strip	6 ~ 15	$9.2 \times 10^2 \sim 6.5 \times 10^4$

Moreover, when the copper liquid contacts the mold wall or the surface of the casting roller, these interfaces can be used as the matrix of non-uniform nucleation to form the embryo. For non-uniform nucleation, it requires less nucleation work, and under smaller undercooling conditions, non-uniform nucleation has a large nucleation rate (Ref 28). Therefore, the solidification structure of the strip is finer under the TRSC.

5. Conclusion

- (1) In DSC experiment, the initial melting temperature of Cu-6Ni-1.4Si alloy was 1048 °C, and the complete melting temperature was 1100 °C. The initial solidification temperature is 1077 °C, and the complete solidification temperature is 1057 °C. The solidification structure is coarse dendrite structure, and there is obvious element segregation at the dendrite boundary.
- (2) During the heating process of CSLM experiment, the initial melting temperature of the alloy was about 1091 °C. In the cooling process of CSLM, the relationship between the crystallization temperature ($T_L \rightarrow s$)

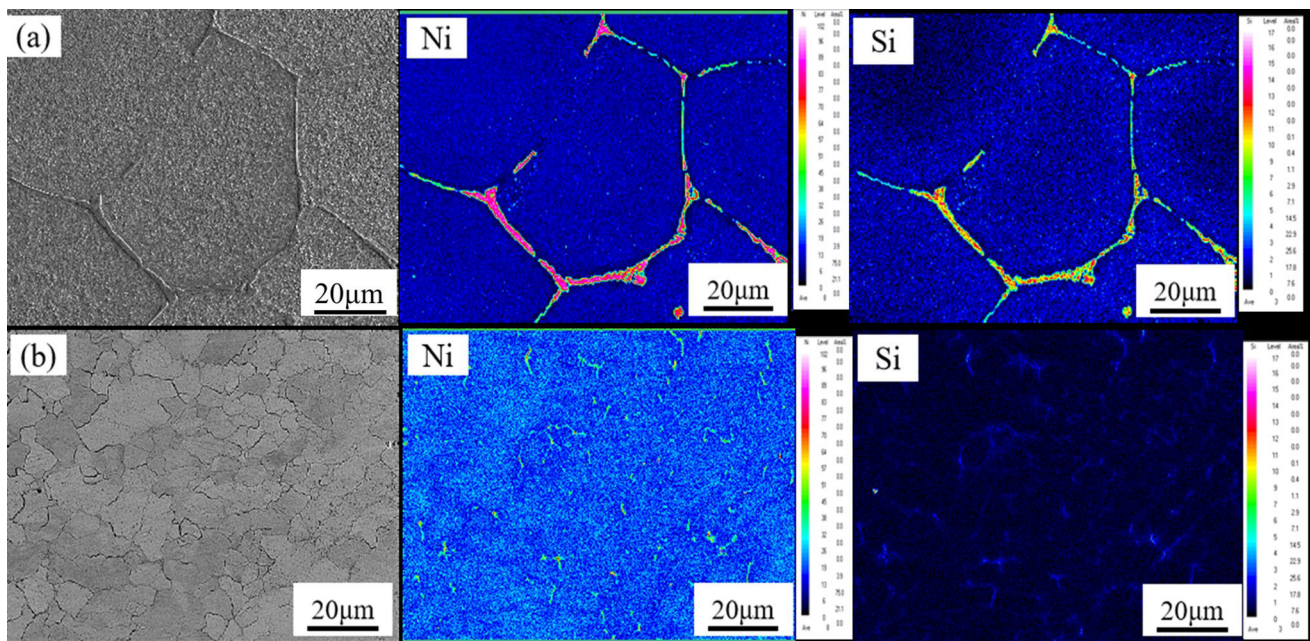


Fig. 8 Elements scanning of ingot and strip microstructure. (a) Ingot; (b) cast strip

and the secondary dendrite arm spacing (λ_2) with the cooling rate is $T_{L \rightarrow S} = 176 \times \exp(-v/17.6) + 891$ and $\lambda_2 = 63 \times v^{-0.236}$, respectively, which decrease with the increase of cooling rate. In addition, the segregation degree of alloy elements in dendritic structure also decreases with the increase of cooling rate.

- (3) Compared with IC, TRSC can significantly refine grains and reduce segregation, which can effectively improve the casting performance of the alloy and provide a good foundation for subsequent processing.

Acknowledgments

This work was supported by the National MCF (Magnetic Confinement Fusion) Energy R&D Program of China (with Grant No. 2018YFE0306102) and the Postdoctoral Science Foundation of China (Grant No. 2021M701167).

References

- Q. Lei, Z. Li, T. Xiao, Y. Pang, Z.Q. Xiang, W.T. Qiu, and Z. Xiao, A New Ultrahigh Strength Cu-Ni-Si Alloy, *J. Intermet.*, 2013, **42**, p 77–84. <https://doi.org/10.1016/j.intermet.2013.05.013>
- Q. Lei, Z. Li, M.P. Wang, L. Zhang, Z. Xiao, and Y.L. Jia, The Evolution of Microstructure in Cu-8.0 Ni-1.8 Si-0.15 Mg Alloy During Aging, *Mater. Sci. Eng. A*, 2010, **527**(24–25), p 6728–6733. <https://doi.org/10.1016/j.msea.2010.07.023>
- Z.Y. Pan, M.P. Wang, Z. Li, Z. Xiao, and C. Chen, Thermomechanical Treatment of Super High Strength Cu-8.0Ni-1.8Si Alloy, *Trans. Nonferrous Met. Soc. China*, 2007, **17**, p 1076–1080
- Q. Dong, D. Zhao, P. Liu, B.K. Kang, and J.L. Huang, Microstructural Changes of Cu-Ni-Si Alloy During Aging, *J. Mater. Sci. Technol.*, 2004, **20**, p 99–102
- Z. Rdzawski and J. Stobrawa, Thermomechanical Processing of Cu-Ni-Si-Cr-Mg Alloy, *Mater. Sci. Technol.*, 1993, **2**(12), p 142–145. <https://doi.org/10.1179/026708393790171836>
- K.M. Sun, L. Li, S.D. Chen, G.M. Xu, G. Chen, R.D.K. Misra, and G. Zhang, A New Approach to Control Centerline Macrosegregation in Al-Mg-Si Alloys During Twin Roll Continuous Casting, *Mater. Lett.*, 2017, **190**, p 205–208. <https://doi.org/10.1016/j.matlet.2016.12.109>
- G.M. Cao, S. Zhang, J. Chen, F. Jia, F. Fang, and C.G. Li, Microstructure and Precipitate Evolution in Cu-3.2Ni-0.75Si Alloy Processed by Twin-Roll Strip Casting, *J. Mater. Eng. Perform.*, 2021, **30**(2), p 1318–1329. <https://doi.org/10.1007/s11665-020-05371-y>
- Z.Y. Liu, Z.S. Lin, S.H. Wang, Y.Q. Qiu, X.H. Liu, and G.D. Wang, Microstructure Characterization of Austenitic Fe-25Mn-22Cr-2Si-0.7N Alloy Processed by Twin Roll Strip Casting, *Mater. Charact.*, 2007, **58**, p 974–979. <https://doi.org/10.1016/j.matchar.2006.10.005>
- M. Daamen, C. Haase, J. Dierdorf, D.A. Molodov, and G. Hirt, Twin-Roll Strip Casting: A Competitive Alternative for the Production of High-Manganese Steels with Advanced Mechanical Properties, *Mater. Sci. Eng. A*, 2015, **627**, p 72–81. <https://doi.org/10.1016/j.msea.2014.12.069>
- K.S. Pandey, S.K. Pandey, and P. Premkumar, Effect of Cooling Rates on Dendritic Arm Spacing and Hardness of Zn-12%, Al-0.3% Cu Alloy, *Indian Foundry J*, 1979, **25**(12), p 29–32
- M.J. Behnam, P. Davami, and N. Varahram, Effect of Cooling Rate on Microstructure and Mechanical Properties of Gray Cast Iron, *Mater. Sci. Eng. A*, 2010, **528**(2), p 583–588. <https://doi.org/10.1016/j.msea.2010.09.087>
- E. Wielgosz and T. Kargul, Differential Scanning Calorimetry Study of Peritectic Steel Grades, *J. Therm. Anal. Calorim.*, 2015, **119**, p 1547–1553. <https://doi.org/10.1007/s10973-014-4302-5>
- Z.J. Miao, A.D. Shan, W. Wang, J. Lu, W.L. Xu, and H.W. Song, Solidification Process of Conventional Superalloy by Confocal Scanning Laser Microscope, *Trans. Nonferrous Met. Soc.*, 2011, **21**(2), p 236–242. [https://doi.org/10.1016/S1003-6326\(11\)60704-8](https://doi.org/10.1016/S1003-6326(11)60704-8)

- K. Hechu, C. Slater, B. Santillana, S. Clark, and S. Sridhar, A Novel Approach for Interpreting the Solidification Behaviour of Peritectic Steels by Combining CSLM and DSC, *Mater. Charact.*, 2017, **133**, p 25–32. <https://doi.org/10.1016/j.matchar.2017.09.013>
- P.H. Nicácio, A.M. Severo, A.B. Barros, A.K. Albuquerque, R.M. Wellen, and K. Koschek, Approaches on the Complex Crystallization in PLA/Babassu Based on Modulated Differential Scanning Calorimetry Analyses, *J. Polym. Environ.*, 2022, **30**(9), p 3840–3851. <https://doi.org/10.1007/s10924-022-02468-4>
- J.Y. Cheng, B.B. Tang, F.X. Yu, and B. Shen, Evaluation of Nanoscaled Precipitates in a Cu-Ni-Si-Cr Alloy During Aging, *Alloys Compd.*, 2014, **614**, p 189–195. <https://doi.org/10.1016/j.jallcom.2014.06.089>
- Y.S. Hao, J. Li, X. Li, W.C. Liu, G.M. Cao, C.G. Li, and Z.Y. Liu, Influences of Cooling Rates on Solidification and Segregation Characteristics of Fe-Cr-Ni-Mo-N Super Austenitic Stainless Steel, *J. Mater. Process. Technol.*, 2019, **275**, p 116326. <https://doi.org/10.1016/j.jmatprotec.2019.116326>
- Y. Xu, N. Ellendt, X.G. Li, V. Uhlenwinkel, and U. Fritsching, Characterization of Cooling Rate and Microstructure of CuSn Melt Droplet in Drop on Demand Process, *Trans. Nonferrous Met. Soc. China*, 2017, **27**(7), p 1636–1644. [https://doi.org/10.1016/S1003-6326\(17\)60186-9](https://doi.org/10.1016/S1003-6326(17)60186-9)
- J.W. Elmer, S.M. Allen, and T.W. Eagar, Microstructural Development During Solidification of Stainless-Steel Alloys, *Metall. Mater. Trans. A*, 1989, **20**(10), p 2117–2131. <https://doi.org/10.1007/BF02650298>
- J.H. Perepezko and G. Wilde, Melt Undercooling and Nucleation Kinetics, *Curr. Opin. Solid St. M*, 2016, **20**, p 3–12. <https://doi.org/10.1016/j.cossms.2015.07.001>
- M. Gholami, I. Altenberger, J. Vesely, H.A. Kuhn, M. Wollmann, M. Janacek, and L. Wagner, Effects of Severe Plastic Deformation on Transformation Kinetics of Precipitates in CuNi3Si1Mg, *Mater. Sci. Eng. A*, 2016, **676**, p 156–164. <https://doi.org/10.1016/j.msea.2016.08.099>
- L.S. Tian, Y.C. Guo, J.P. Li, F. Xia, M.X. Liang, and Y.P. Bai, Effects of Solidification Cooling Rate on the Microstructure and Mechanical Properties of a Cast Al-Si-Cu-Mg-Ni Piston Alloy, *Adv. Mater.*, 2018 <https://doi.org/10.3390/ma11071230>
- X. Li, F. Gao, J.H. Jiao, G.M. Cao, Y. Wang, and Z.Y. Liu, Influences of Cooling Rates on Delta Ferrite of Nuclear Power 316H Austenitic Stainless Steel, *Mater. Charact.*, 2021, **174**, p 111029. <https://doi.org/10.1016/j.matchar.2021.111029>
- E. Wielgosz and T. Kargul, Differential Scanning Calorimetry Study of Peritectic Steel Grades, *J. Therm. Anal. Calorim.*, 2015, **119**, p 1547–1553. <https://doi.org/10.1007/s10973-014-4302-5>
- Y.M. Won and B.G. Thomas, Simple Model of Microsegregation During Solidification of Steels, *Metall. Mater. Trans. A*, 2001, **32**, p 1755–1767. <https://doi.org/10.1007/s11661-001-0152-4>
- H.T. Liu, Z.H. Liu, Y.Q. Qiu, G.M. Cao, C.C. Li, and G.D. Wang, Characterization of the Solidification Structure and Texture Development of Ferritic Stainless Steel Produced by Twin-roll Strip Casting, *Mater. Charact.*, 2009, **60**(1), p 79–82. <https://doi.org/10.1016/j.matchar.2008.06.005>
- G. Li, W. Yu, and Q. Cai, Investigation of Reduction Pretreatment Process for Continuous Casting, *J. Mater. Process. Technol.*, 2016, **227**, p 41–48. <https://doi.org/10.1016/j.jmatprotec.2015.08.005>
- T. Xiao, X.F. Sheng, Q. Lei, J.L. Zhu, S.Y. Li, Z.R. Liu, and Z. Li, Effect of Magnesium on Microstructure Refinements and Properties Enhancements in High-Strength Cu-Ni-Si Alloys, *Acta Metall. Sin. (Engl. Lett.)*, 2020, **33**, p 375–384. <https://doi.org/10.1007/s40195-019-00953-9>

Publisher's Note Springer Nature remains neutral with regard to jurisdictional claims in published maps and institutional affiliations.

Springer Nature or its licensor (e.g. a society or other partner) holds exclusive rights to this article under a publishing agreement with the author(s) or other rightsholder(s); author self-archiving of the accepted manuscript version of this article is solely governed by the terms of such publishing agreement and applicable law.